Thin-film composite membranes with mineralized nanofiber supports for highly efficient nanofiltration

Yan Lv [a],[*],[1], Jingjing Xia [a],[1], Yang Yang [a], Yizhou Chen [a], Tianxi Liu [a],[b]

[a] State Key Laboratory for Modification of Chemical Fibers and Polymer Materials, Innovation Center for Textile Science and Technology, College of Materials Science and Engineering, Donghua University, 2999 North Renmin Road, Shanghai, 201620, PR China
[b] Key Laboratory of Synthetic and Biological Colloids, Ministry of Education, School of Chemical and Material Engineering, Jiangnan University, Wuxi, 214122, PR China

ABSTRACT

Nanofiltration has exhibited broad application prospects in the field of precise separation attributed to its unique sieving performance for ions and small molecules, high permeation flux and low energy consumption. However, it remains a great challenge for current nanofiltration membranes (NFMs) to improve the permeability while maintaining the high rejection for divalent (or multivalent) ions. In this work, we design and fabricate a novel thin-film composite (TFC) nanofiltration membrane, for which an electrospun polyacrylonitrile nanofiber membrane is adopted as the support after modified by a zirconia mineral layer via surface biomimetic mineralization method, and then an ultrathin selective layer of polyamide (PA) with wrinkled structure is constructed on it via interfacial polymerization. The hydrophilic mineralized nanofiber surface can help to decrease the thickness of the PA layer significantly. Meanwhile, the abundant zirconia particles acting as templates will generate a wrinkled structure for PA layer, providing an improved effective filtration area. Therefore, the resultant NFMs exhibit a high water flux of 38.2 L m^{-2} h^{-1} (under 4 bar) accompanied with excellent rejection rate for divalent anions (e.g. 97.6% for SO$_4^{2-}$) and cations (e.g. 92.4% for Mg^{2+}). This study could pave an avenue to develop highly efficient NFMs for comprehensive separation applications.

Membrane technology has become one of the most important separation processes nowadays due to the merits of high efficiency, low energy consumption, and free of secondary pollution compared with many traditional industrial methods such as distillation, extraction, flocculation, and so on [1–3]. Nanofiltration, as an emerging and promising membrane technology, has attracted extensive attention during the last decades attributed to the unique separation characteristics of high selective rejection for multivalent (or divalent) ions and dissolved small organic molecules (200–2000 Da) with excellent permeate flux [4,5]. Therefore, it is widely applied in desalination, surface water purification and wastewater reclamation to help alleviate the water crisis [6].

Most state-of-the-art nanofiltration membranes (NFMs) possess a thin-film composite structure composed of a dense selective layer and a porous substrate layer [5]. The selective layer is generally polyamide (PA) fabricated via interfacial polymerization (IP) between amine and acyl chloride monomers, which dominantly determines the membrane separation performance. Meanwhile, the substrate can not only provide mechanical support and solvent transport channels, but also influence the structures and properties of selective layers [7–11]. So it is the key to optimize the composite membrane structures for improving the nanofiltration performance [13]. On the one hand, tremendous efforts have been conducted to reduce the thickness of the skin layer and regulate its morphology and structure [5]. For example, Livingston et al. [14] introduced a sacrificial layer of cadmium hydroxide nanowire onto the support surface to store the aqueous monomer solution and control their release to the organic-water interface, resulting in ultra-thin PA layer with ultra-high permeate flux in organic solvent nanofiltrations. Xu and co-workers found that hydrophilic interlayers via co-deposition of polyphenols or polydopamine (PDA) with amines would control the PA thickness and simultaneously enhance the interfacial interaction between the PA layer and the substrate [15,16]. In order to tune the morphologies of PA layers on nanoscale, Gao et al. [17] added poly (vinyl alcohol) into the aqueous solutions as co-reactant and achieved

---
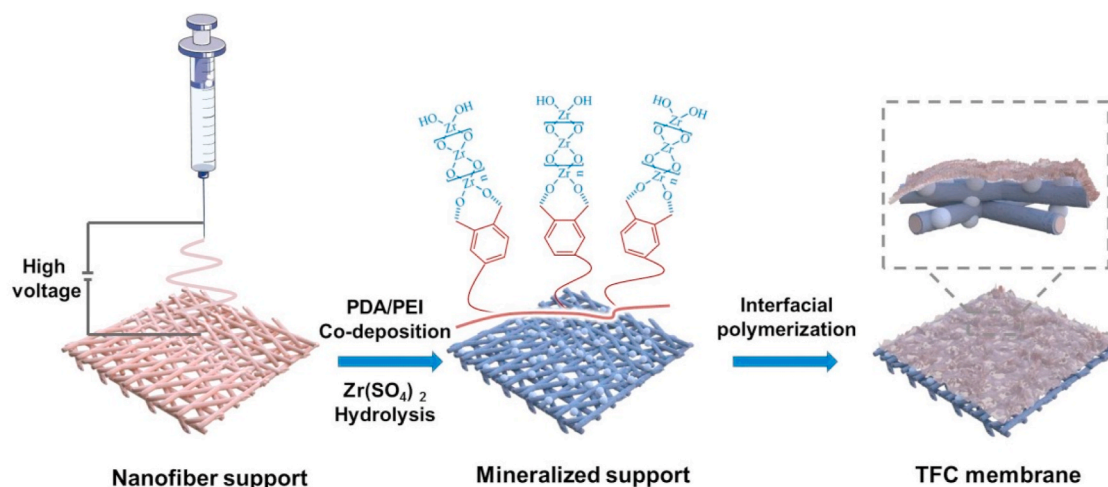
Scheme 1. Schematic illustration of the fabrication process for the composite NFMs with mineralized nanofiber supports.

high salt rejection with good permeation flux. Jin et al. [18] synthesized zeolitic imidazolate framework (ZIF) nanoparticles onto an interlayer of multi-walled carbon nanotubes as templates to facilitate the formation of crumpled structures for the PA layer, realizing an improved water flux without sacrificing the rejection performance. On the other hand, researchers tried to adopt micro-porous membranes as supports instead of traditional asymmetrical ultrafiltration (UF) membranes to shorten the lateral travel distance for water molecules and reduce the trans-membrane hydraulic resistance and thus further improve the flux [19–21]. Xu et al. [22] fabricated selective layers on a series of micro-filtration membranes with hydrophilic coatings to achieve high water permeability. In comparison, nanofiber membranes with higher porosity, larger pore size and lower tortuosity seem to be better candidates as supports for NFMs [23,24]. Sun and co-workers prepared a PA layer with a thickness of around 150 nm on a cross-linked poly-acrylonitrile (PAN) nanofiber support for organic solvent nanofiltration with improved permeability [25]. However, interlayers including gelatin, cellulose or even loose PA layers are usually adopted to reduce the surface pore size of the nanofiber supports and thus guarantee the integrity and reduce the thickness of selective layers [26–28]. Clearly, it is a great challenge to construct ultra-thin and defect-free selective layers on microporous nanofiber supports directly, restricting the
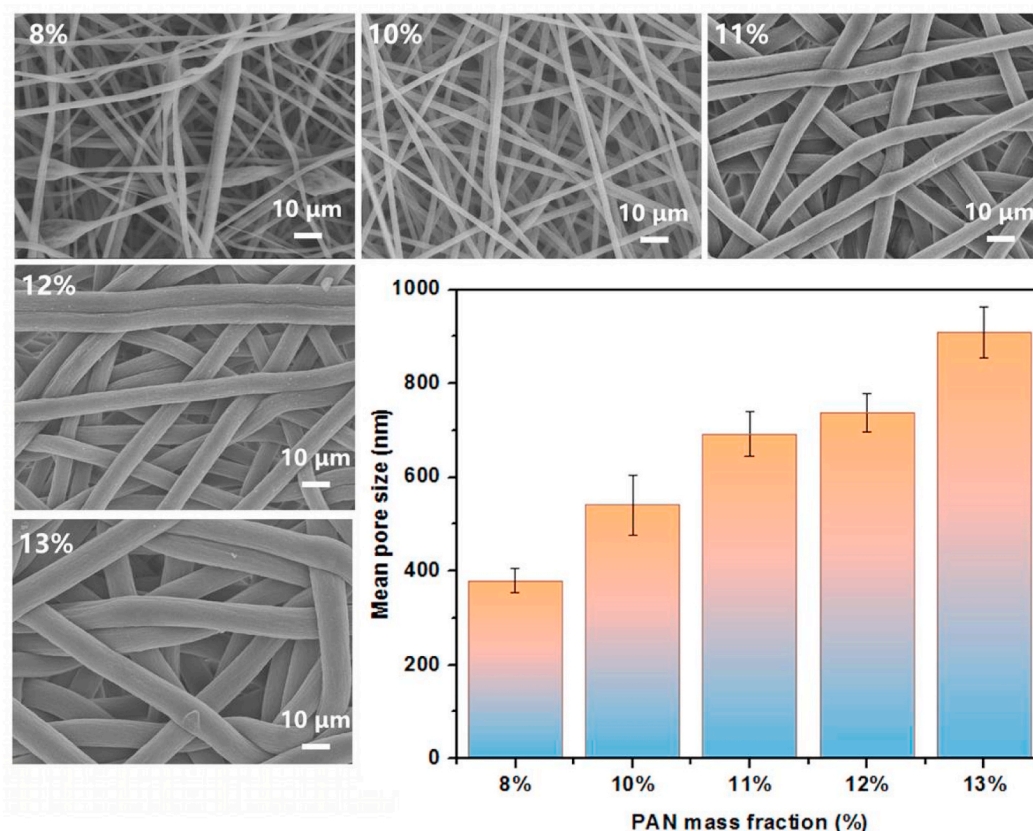
Fig. 1. SEM images of nanofiber membranes prepared using electrospinning solutions with different PAN concentrations (in mass fraction), and the corresponding mean pore sizes.
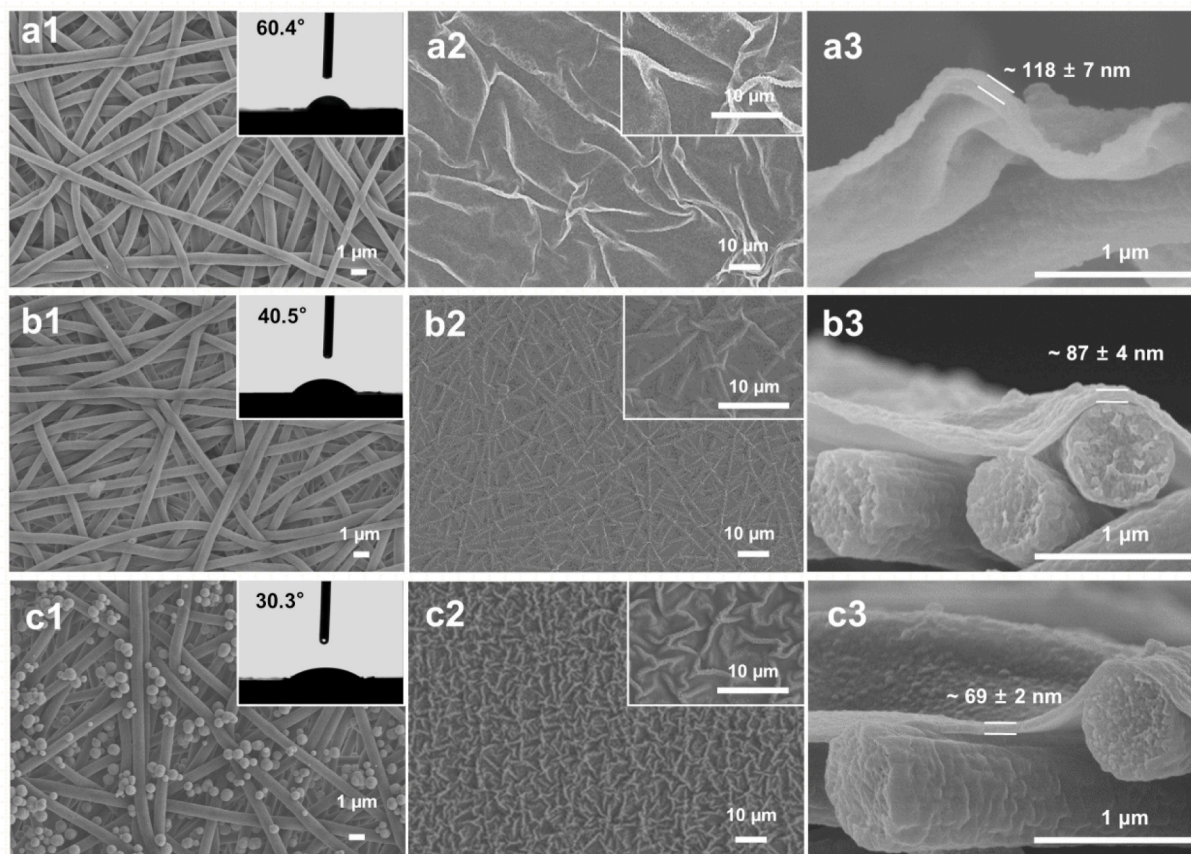
Fig. 2. SEM images of different membrane surfaces and cross sections. a1) Pristine NFS and a2-a3) composite membranes prepared via IP on pristine NFSs. b1) PNFS and b2-b3) composite membranes prepared via IP on PNFSs. c1) ZNFS and c2-c3) composite membranes prepared via IP on ZNFSs. The inserts in a1), b1) and c1) show the water contact angles of the support surfaces.

superiorities of the unique nanofibrous structures.

Herein, we demonstrate a novel TFC NFM with a mineralized nanofiber support for high-efficiency ion sieving with enhanced water flux. As shown in Scheme 1, the nanofiber support is prepared by electrospinning using PAN solution. Then the nanofibers in the support are modified by PDA/polyethyleneimine (PEI) coatings, which further induce surface mineralization with zirconia coatings via hydrolysis of zirconium ions (Zr^{4+}) according to our previous work [29,30]. Finally, interfacial polymerization between piperazine hexahydrate (PIP) and trimesoyl chloride (TMC) is conducted on the mineralized nanofiber support to form a PA selective layer. The nanofiber supports could provide affluent transport channels for water with low hydraulic resistance. Zirconia is adopted to modify the support surface to improve the hydrophilicity, which can help to control the release of PIP to the reaction interface and thus reduce the PA thickness. Moreover, the abundant zirconia particles on the mineral coatings can act as templates to generate abundant wrinkles for the PA layer, resulting in increased effective filtration area. As a result, the prepared NFMs will exhibit excellent water flux compared with that using commercial UF supports. Interestingly, the NFMs could reject both divalent anions and cations effectively, attributing to the synergistically electrostatic repulsion of the defect-free selective layers with negative charges and the positively charged support surfaces. This work can provide a facile strategy to develop next-generation composite NFMs for rapid and highly selective ionic separations.

As the porous structure of the supports has significant effects on the IP process and the resultant PA layers [8], the nanofiber supports are firstly optimized by adjusting the PAN concentration in electrospinning solutions. It can be observed from the scanning electron microscopy (SEM) images in Fig. 1 that the nanofiber diameter increases with PAN

concentrations because of the increased solution viscosity and surface tension impeding the split of nanofibers (Fig. S1). Especially, at a low PAN concentration of 8 wt%, the nanofiber diameter distribution is uneven with lots of beads. However, the nanofiber diameter becomes uniform when the PAN concentration increases from 10 wt% to 13 wt% accompanied with improved mean pore size of the nanofiber membranes. We applied nanofiber membranes with different pore sizes for the fabrication of TFC membranes and found that the composite membranes using nanofiber supports with moderate pore size showed the best separation performance (Fig. S2). This is because the amount of PIP solution stored in supports with small pore size might be insufficient for IP reaction to form dense PA layers with high crosslinking degree. And for supports with large pore size, the PIP solution would distribute unevenly on the support surface, resulting in defects for PA layers and thus unsatisfactory rejection performance [5,8,12]. Therefore, the PAN concentration is optimized at 12 wt% for electrospinning in consideration of the uniform nanofiber diameter, the appropriate pore size and the stable structures.

Fig. 2 displays the morphologies of different nanofiber supports before and after interfacial polymerization. The pristine PAN nanofiber support (NFS) is fully covered by a dense and uneven PA layer with a thickness of about 118 nm. The surface morphology changes little for the PDA/PEI modified nanofiber support (PNFS) as the conformal ultra-thin PDA/PEI coating can be deposited on the nanofiber surface uniformly. However, the PA layer formed on the PNFS is more wrinkled with a reduced thickness of ~87 nm. This should be attributed to the much hydrophilic support surface that can store more aqueous solutions and control the uniform release of PIP to the interfacial reactive zone [14, 31]. After mineralization, the nanofiber diameter increases slightly but the support still maintains microporous structures well with a mean pore
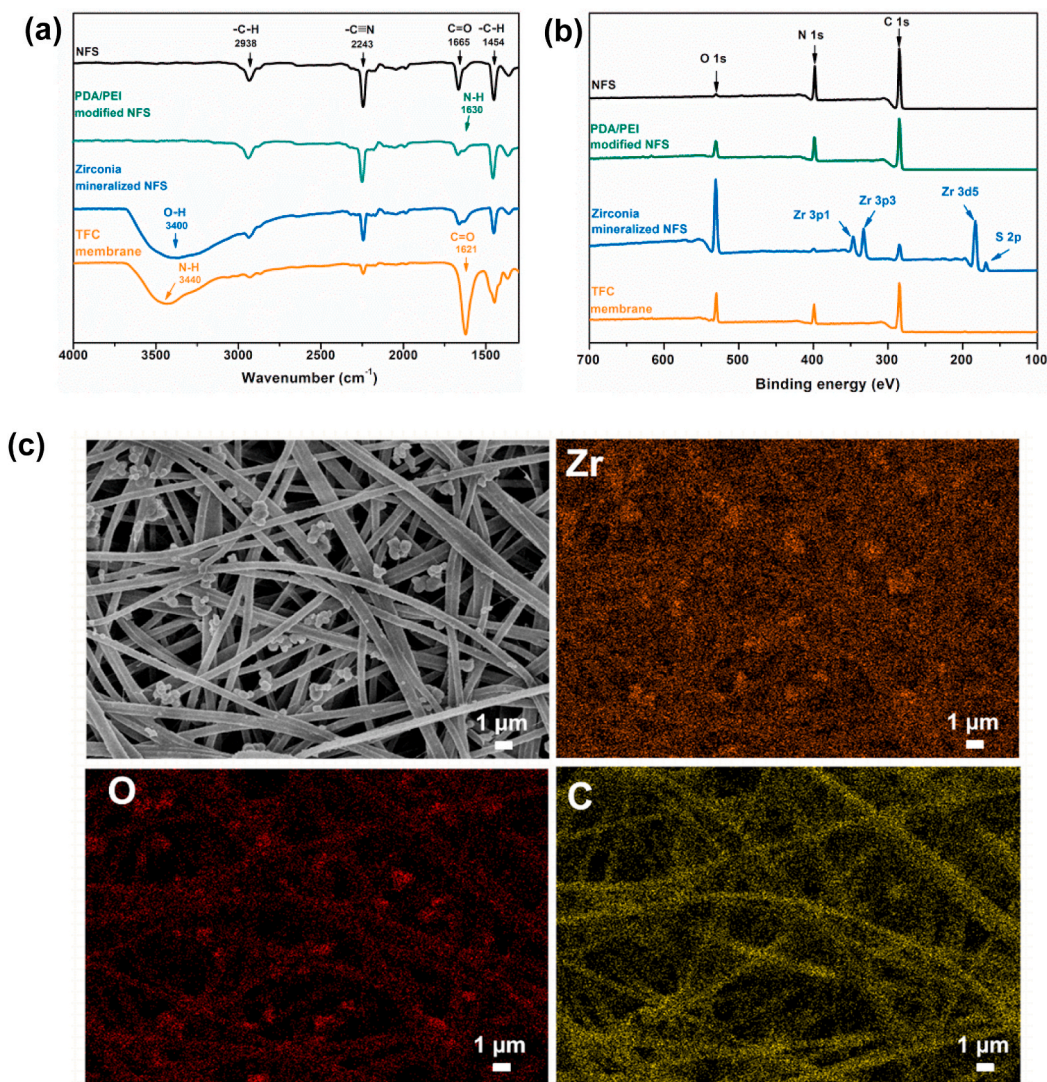
Fig. 3. a) FTIR and b) XPS spectra of different membrane surfaces. c) SEM and EDS images of the ZNFS surface showing the element distribution.

Table 1
Element compositions of different membrane surfaces calculated from XPS spectra (in atomic percent).

Sample	C (%)	O (%)	N (%)	Zr (%)	C/O
PAN NFS	65.03	3.55	31.23	0	18.31
PDA/PEI modified NFS	56.50	19.71	23.79	0	2.87
Zirconia mineralized NFS	11.12	48.83	2.44	34.33	0.23
TFC membrane	53.88	28.43	17.69	0	1.89

size of about 0.7 μm (Table S1). As the surface hydrophilicity is further improved, the zirconia decorated nanofiber support could slow down the migration rate of PIP to the water-organic interface [33,34]. As a result, the thickness of the PA layer is reduced to ~69 nm. Meanwhile, the abundant zirconia nanoparticles generated on the ZNFS surface can act as templates to promote the formation of serried wrinkles for the PA layer, resulting in enlarged effective filtration area that will benefit the membrane permeate flux.

The chemical structures and compositions were analyzed in detail by attenuated total reflectance Fourier transform infrared (FTIR/ATR) spectrometer and X-ray photoelectron spectrometer (XPS), respectively. From Fig. 3a, the FTIR spectrum of the pristine nanofiber support exhibits characteristic vibration peaks of C≡N (2243 cm^{-1}), C–H (2938

cm^{-1}, 1454 cm^{-1}) in PAN and C=O (1665 cm^{-1}) derived from the additives. For the PNFS samples, new peaks appear at 1630 cm^{-1} and 1656 cm^{-1} related to the N–H bond vibration in amine groups of PDA and PEI. After mineralization, the broad peak at 3400 cm^{-1} becomes significant while other peaks weaken ascribed to the abundant hydroxy groups in zirconia coating on the PNFS nanofibers. For the TFC membrane, new peaks corresponding to the stretching vibration of C=O and bending vibration of N–H in amide groups rise at 1621 cm^{-1} and 3440 cm^{-1}, respectively, indicating the formation of a PA layer. In the XPS spectra of NFS and PNFS, only C, N and O were detected with C/O ratio of 18.31 and 2.87, respectively (Fig. 3b, Table 1). This is because the PDA/PEI layer contains abundant hydroxy groups. A new element of Zr is detected on the ZNFS surface accompanied with further decreased C/O ratio due to the formation of zirconia coatings. Furthermore, the distribution of zirconia on the ZNFS surface can be observed by energy dispersive X-ray spectroscopy (EDX). As shown in Fig. 3c, the nanofibers are coated by zirconia minerals, and the chemical composition of the nanoparticles adhered on the support surface is also verified to be zirconia. Finally, after IP process, the XPS signal of Zr element disappears and the C/O ratio recovers to 1.89 because the support surface is covered by a PA layer.

The membrane surface properties are crucial for the comprehensive separation performance [32]. Water contact angles of different membrane surfaces were measured to evaluate the wetting property (Fig. 4a).
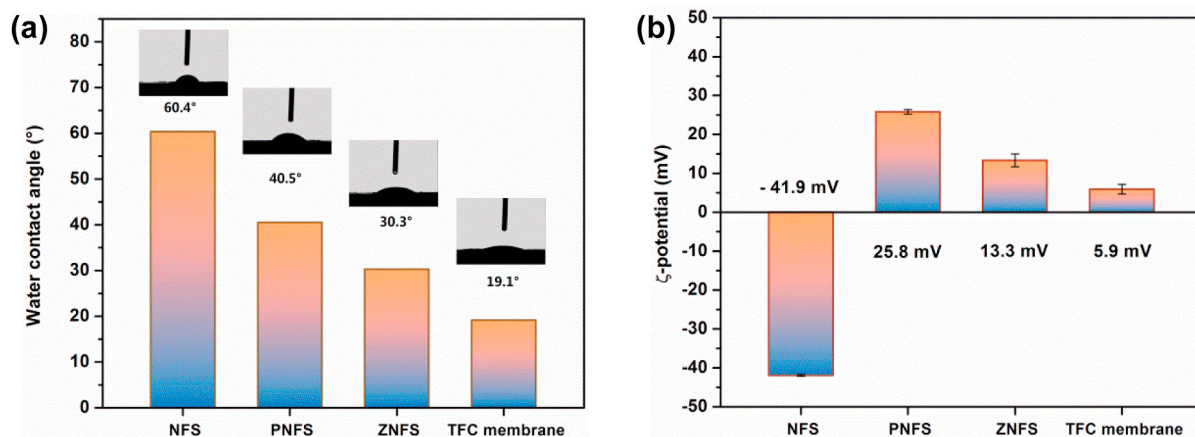
Fig. 4. a) Water contact angles and b) ζ-potentials (under pH 6.0) of different membrane surfaces.
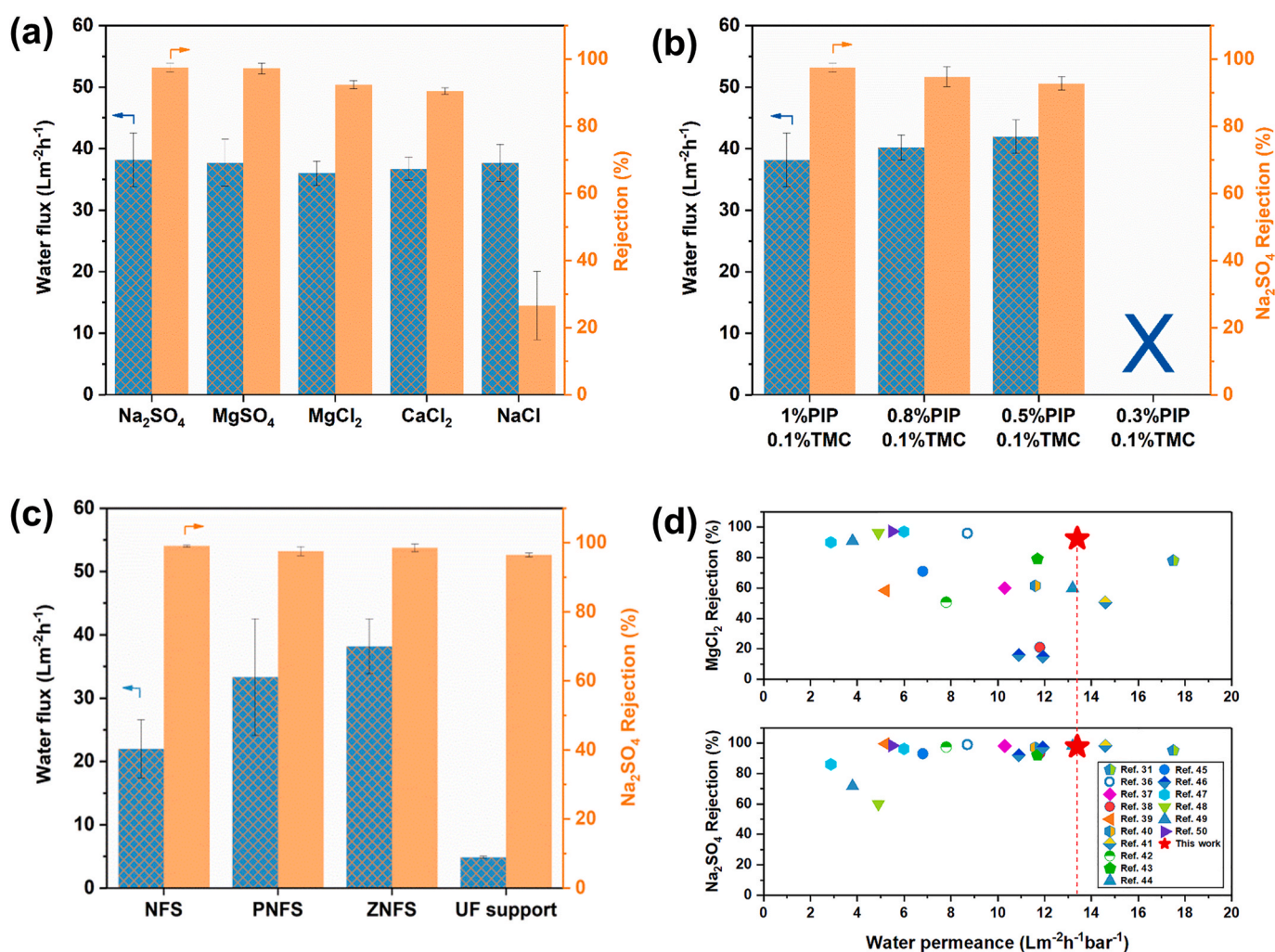
Fig. 5. a) Nanofiltration performances of composite NFMs prepared with different nanofiber and commercial UF supports. b) Effects of monomer concentrations in IP processes on the NFM separation performances. c) Nanofiltration performances of the optimized composite NFMs for different salt solutions. d) Performance comparison of the prepared NFMs with those reported in literatures [31,36–50].

The water contact angle of the pristine NFS surface is about 60.4°. The value decreases to 40.5° for the PNFS because of the good hydrophilicity of the PDA/PEI coating. After mineralization, the inorganic zirconia coating with abundant nanoparticles endows the ZNFS surface with

further enhanced wettability. Though the membrane surface becomes dense after IP, the wrinkled morphologies and rich hydrophilic groups (carboxyl and amide) endow the membrane with further improved wettability, which is beneficial for the water flux and anti-fouling

performance. The charged property of membrane surfaces determines the rejection for charged solutes according to the Donnan effect. As shown in Fig. 4b, the pristine NFS surface is negatively charged, which converts to positive after PDA/PEI modification due to the protonation of amine groups in the coatings. As the zirconia coating with slight positive charges is thin, the ζ-potential of ZNFS surface maintains positive at around 13.3 mV. The PA surface is usually negatively charged attributed to the ionized carboxyl groups, leading to decreased ζ-potential to 5.9 mV for the TFC membrane surface. The unique composite structure of positively charged support and negatively charged selective layer may bestow unconventional separation performance for ions to the TFC membrane.

The separation performance of TFC membranes with different supports for Na_2SO_4 solutions was evaluated. It can be seen in Fig. 5a that all of the membranes exhibit similar high rejection (>97%) for Na_2SO_4 owing to the defect-free PA layers with negative charges. However, the water flux increases from 21.5 L m^{-2} h^{-1} for membranes with pristine NFSs to 38.2 L m^{-2} h^{-1} for membranes with ZNFSs. The enhanced water flux should be attributed to the reduced thickness of PA layers and the enlarged effective filtration area derived from the wrinkled morphologies. In contrast, the TFC membranes with commercial UF supports reveal a water flux of 4.8 L m^{-2} h^{-1}, which is about 8 times lower than that of the membranes with ZNFSs. Furthermore, the separation performance is optimized by adjusting the IP conditions. The water flux increases slightly with decreased PIP concentration while the rejection rate declines ascribed to the inadequate crosslink reaction and the loose structure of the PA layers. The PA layer becomes fragmentary and invalid for salt rejection when the PIP concentration reaches to 0.3% (Fig. S3). The optimized NFMs were applied in the treatment of different salt solutions. The water fluxes vary little for different dilute salt solutions as their osmotic pressures are similar. Interestingly, the NFMs exhibit high rejection for both divalent anions (e.g. 97.6% for Na_2SO_4, 97.2% for $MgSO_4$) and cations (e.g. 92.4% for $MgCl_2$, 91.5% for $CaCl_2$), which is significantly different from conventional TFC membranes prepared by IP method. This is because the anions can be rejected by the dense negatively charged PA layer while the cations can be repelled by the positively charged support surface when they are passing through the PA layer. This synergistic repulsion effect of a dually charged composite membrane surface was preliminarily proved in literatures [35, 36]. Meanwhile, the TFC membranes show low rejection (~27%) for NaCl ascribed to the small hydrated radius of Na$^+$ (0.358 nm) and Cl$^-$ (0.332 nm) as well as the weak electrostatic repulsion between the membrane surface and divalent ions. This result indicates that the NFMs possess good selective separation performance for monovalent ions and divalent ions. All in all, the prepared NFMs show relatively competitive comprehensive separation performance compared with previously reported and commercial composite NFMs (Fig. 5d, Table S2).

In summary, we have developed a novel composite nanofiltration membrane via interfacial polymerization on a mineralized nanofiber support. On the one hand, the nanofiber supports with micro-sized pores, high porosity and low tortuosity provide adequate channels and shorten the lateral distance for water transport with low hydraulic resistance. On the other hand, the hydrophilic zirconia mineral coating can control the uniform release of PIP monomer to the reactive zone to achieve a thin PA selective layer. Moreover, the abundant zirconia particles would act as templates to generate wrinkles for PA layer to improve the effective filtration area. As a result, the optimized NFMs exhibit a water flux of 38.2 L m^{-2} h^{-1}, which is 8 times higher than that of the TFC membranes using commercial UF supports. Interestingly, the prepared NFMs show excellent rejection for divalent anions (e.g. 97.6% for SO_4^{2-}) and cations (e.g. 92.4% for Mg^{2+}) attributed to the synergistic repulsion effect of the PA layer and the support surface bearing opposite charges. This study suggests a facile strategy for developing composite membranes with nanofiber supports for highly efficient nanofiltration.

References

[1] D.L. Gin, R.D. Noble, Chemistry. Designing the next generation of chemical separation membranes, Science 332 (2011) 674–676.
[2] M.A. Shannon, P.W. Bohn, M. Elimelech, J.G. Georgiadis, B.J. Marinas, A. M. Mayes, Science and technology for water purification in the coming decades, Nature 452 (2008) 301–310.
[3] H.B. Park, J. Kamcev, L.M. Robeson, M. Elimelech, B.D. Freeman, Maximizing the right stuff: the trade-off between membrane permeability and selectivity, Science (2017) 356, eaab0530.
[4] A.W. Mohammad, Y.H. Teow, W.L. Ang, Y.T. Chung, D.L. Oatley-Radcliffe, N. Hilal, Nanofiltration membranes review: recent advances and future prospects, Desalination 356 (2015) 226–254.
[5] H. Zhang, Q. He, J. Luo, Y. Wan, S.B. Darling, Sharpening nanofiltration: strategies for enhanced membrane selectivity, ACS Appl. Mater. Interfaces 12 (2020) 39948–39966.
[6] Z. Yang, P.F. Sun, X. Li, B. Gan, L. Wang, X. Song, H.D. Park, C.Y. Tang, A critical review on thin-film nanocomposite membranes with interlayered structure: mechanisms, recent developments, and environmental applications, Environ. Sci. Technol. 54 (2020) 15563–15583.
[7] W.J. Lau, A.F. Ismail, N. Misdan, M.A. Kassim, A recent progress in thin film composite membrane: a review, Desalination 287 (2012) 190–199.
[8] X. Li, Q. Li, W. Fang, R. Wang, W.B. Krantz, Effects of the support on the characteristics and permselectivity of thin film composite membranes, J. Membr. Sci. 580 (2019) 12–23.
[9] G.-R. Xu, J.-M. Xu, H.-J. Feng, H.-L. Zhao, S.-B. Wu, Tailoring structures and performance of polyamide thin film composite (PA-TFC) desalination membranes via sublayers adjustment-a review, Desalination 417 (2017) 19–35.
[10] Y.-H. Pan, Q.-Y. Zhao, L. Gu, Q.-Y. Wu, Thin film nanocomposite membranes based on imologite nanotubes blended substrates for forward osmosis desalination, Desalination 421 (2017) 160–168.
[11] S.-J. Shi, Y.-H. Pan, S.-F. Wang, Z.-W. Dai, L. Gu, Q.-Y. Wu, Aluminosilicate nanotubes embedded polyamide thin film nanocomposite forward osmosis membranes with simultaneous enhancement of water permeability and selectivity, Polymers (2019) 11.
[12] X. Zhang, C. Liu, J. Yang, C.-Y. Zhu, L. Zhang, Z.-K. Xu, Nanofiltration membranes with hydrophobic microfiltration substrates for robust structure stability and high water permeation flux, J. Membr. Sci. 593 (2020) 117444.
[13] Q.-Y. Wu, X.-Y. Xing, Y. Yu, L. Gu, Z.-K. Xu, Novel thin film composite membranes supported by cellulose triacetate porous substrates for high-performance forward osmosis, Polymer 153 (2018) 150–160.
[14] Z.J. Santanu Karan, Andrew G. Livingston, Sub–10 nm polyamide nanofilms with ultrafast solvent transport for molecular separation, Science 348 (2015) 1347–1351.
[15] X. Zhang, Y. Lv, H.C. Yang, Y. Du, Z.K. Xu, Polyphenol coating as an interlayer for thin-film composite membranes with enhanced nanofiltration performance, ACS Appl. Mater. Interfaces 8 (2016) 32512–32519.
[16] X. Yang, Y. Du, X. Zhang, A. He, Z.K. Xu, Nanofiltration membrane with a mussel-inspired interlayer for improved permeation performance, Langmuir 33 (2017) 2318–2324.
[17] S.C. Zhe Tan, Xinsheng Peng, Lin Zhang, Congjie Gao, polyamide membranes with nanoscale turing structures for water purification, Science 360 (2018) 518–521.
[18] Z. Wang, Z. Wang, S. Lin, H. Jin, S. Gao, Y. Zhu, J. Jin, Nanoparticle-templated nanofiltration membranes for ultrahigh performance desalination, Nat. Commun. 9 (2018) 2004.
[19] Z. Jiang, S. Karan, A.G. Livingston, Water transport through ultrathin polyamide nanofilms used for reverse osmosis, Adv. Mater. 30 (2018) 1705973.

[20] W.-J. Lau, G.-S. Lai, J. Li, S. Gray, Y. Hu, N. Misdan, P.-S. Goh, T. Matsuura, I. W. Azelee, A.F. Ismail, Development of microporous substrates of polyamide thin film composite membranes for pressure-driven and osmotically-driven membrane processes: a review, J. Ind. Eng. Chem. 77 (2019) 25–59.

[21] L. Meng, F. Niu, P. Deng, N. Li, Y. Lv, M. Huang, Electrospun nanofiber supports with bio-inspired modification enabled high-performance forward osmosis composite membranes, Compos. Commun. 22 (2020) 100473.

[22] X. Zhang, C. Liu, J. Yang, C.-Y. Zhu, L. Zhang, Z.-K. Xu, Nanofiltration membranes with hydrophobic microfiltration substrates for robust structure stability and high water permeation flux, J. Membr. Sci. 593 (2020) 117444.

[23] Y. Liao, C.-H. Loh, M. Tian, R. Wang, A.G. Fane, Progress in electrospun polymeric nanofibrous membranes for water treatment: fabrication, modification and applications, Prog. Polym. Sci. 77 (2018) 69–94.

[24] H. Saleem, L. Trabzon, A. Kilic, S.J. Zaidi, Recent advances in nanofibrous membranes: Production and applications in water treatment and desalination, Desalination 478 (2020) 114178.

[25] T.-D. Lu, B.-Z. Chen, J. Wang, T.-Z. Jia, X.-L. Cao, Y. Wang, W. Xing, C.H. Lau, S.-P. Sun, Electrospun nanofiber substrates that enhance polar solvent separation from organic compounds in thin-film composites, J. Mater. Chem. A 6 (2018) 15047–15056.

[26] K. Shen, C. Cheng, T. Zhang, X. Wang, High performance polyamide composite nanofiltration membranes via reverse interfacial polymerization with the synergistic interaction of gelatin interlayer and trimesoyl chloride, J. Membr. Sci. 588 (2019) 117192.

[27] X. Wang, T.-M. Yeh, Z. Wang, R. Yang, R. Wang, H. Ma, B.S. Hsiao, B. Chu, Nanofiltration membranes prepared by interfacial polymerization on thin-film nanofibrous composite scaffold, Polymer 55 (2014) 1358–1366.

[28] S. Rajesh, Y. Zhao, H. Fong, T.J. Menkhaus, Nanofiber multilayer membranes with tailored nanochannels prepared by molecular layer-by-layer assembly for high throughput separation, J. Mater. Chem. A 5 (2017) 4616–4628.

[29] Y. Lv, H.-C. Yang, H.-Q. Liang, L.-S. Wan, Z.-K. Xu, Novel nanofiltration membrane with ultrathin zirconia film as selective layer, J. Membr. Sci. 500 (2016) 265–271.

[30] Y. Lv, H.-C. Yang, H.-Q. Liang, L.-S. Wan, Z.-K. Xu, Nanofiltration membranes via co-deposition of polydopamine/polyethylenimine followed by cross-linking, J. Membr. Sci. 476 (2015) 50–58.

[31] M.-B. Wu, Y. Lv, H.-C. Yang, L.-F. Liu, X. Zhang, Z.-K. Xu, Thin film composite membranes combining carbon nanotube intermediate layer and microfiltration support for high nanofiltration performances, J. Membr. Sci. 515 (2016) 238–244.

[32] J. Luo, Y. Wan, Effects of pH and salt on nanofiltration—a critical review, J. Membr. Sci. 438 (2013) 18–28.

[33] X. Zhang, S. Xiong, C.-X. Liu, L. Shen, C. Ding, C.-Y. Guan, Y. Wang, Confining migration of amine monomer during interfacial polymerization for constructing thin-film composite forward osmosis membrane with low fouling propensity, Chem. Eng. Sci. 207 (2019) 54–68.

[34] X. Zhang, S. Xiong, C.-X. Liu, L. Shen, S.-L. Wang, W.-Z. Lang, Y. Wang, Smart TFC membrane for simulated textile wastewater concentration at elevated temperature enabled by thermal-responsive microgels, Desalination 500 (2021) 114870.

[35] S. Liu, C. Wu, W.-S. Hung, X. Lu, K.-R. Lee, One-step constructed ultrathin Janus polyamide nanofilms with opposite charges for highly efficient nanofiltration, J. Mater. Chem. A 5 (2017) 22988–22996.

[36] C. Wu, S. Liu, Z. Wang, J. Zhang, X. Wang, X. Lu, Y. Jia, W.-S. Hung, K.-R. Lee, Nanofiltration membranes with dually charged composite layer exhibiting super-high multivalent-salt rejection, J. Membr. Sci. 517 (2016) 64–72.

[37] Y.-S. Guo, Y.-F. Mi, F.-Y. Zhao, Y.-L. Ji, Q.-F. An, C.-J. Gao, Zwitterions functionalized multi-walled carbon nanotubes/polyamide hybrid nanofiltration membranes for monovalent/divalent salts separation, Separ. Purif. Technol. 206 (2018) 59–68.

[38] Y.-J. Tang, Z.-L. Xu, S.-M. Xue, Y.-M. Wei, H. Yang, Improving the chlorine-tolerant ability of polypiperazine-amide nanofiltration membrane by adding NH2-PEG-NH2 in the aqueous phase, J. Membr. Sci. 538 (2017) 9–17.

[39] M.B.M.Y. Ang, Y.-L. Ji, S.-H. Huang, H.-A. Tsai, W.-S. Hung, C.-C. Hu, K.-R. Lee, J.-Y. Lai, Incorporation of carboxylic monoamines into thin-film composite polyamide membranes to enhance nanofiltration performance, J. Membr. Sci. 539 (2017) 52–64.

[40] J. Zheng, M. Li, K. Yu, J. Hu, X. Zhang, L. Wang, Sulfonated multiwall carbon nanotubes assisted thin-film nanocomposite membrane with enhanced water flux and anti-fouling property, J. Membr. Sci. 524 (2017) 344–353.

[41] J. Wang, C. Zhao, T. Wang, Z. Wu, X. Li, J. Li, Graphene oxide polypiperazine-amide nanofiltration membrane for improving flux and anti-fouling in water Purification, RSC Adv. 6 (2016) 82174–82185.

[42] D. Hu, Z.-L. Xu, C. Chen, Polypiperazine-amide nanofiltration membrane containing silica nanoparticles prepared by interfacial polymerization, Desalination 301 (2012) 75–81.

[43] L.-F. Liu, X. Huang, X. Zhang, K. Li, Y.-L. Ji, C.-Y. Yu, C.-J. Gao, Modification of polyamide TFC nanofiltration membrane for improving separation and antifouling properties, RSC Adv. 8 (2018) 15102–15110.

[44] L. Meihong, Y. Sanchuan, Z. Yong, G. Congjie, Study on the thin-film composite nanofiltration membrane for the removal of sulfate from concentrated salt aqueous: preparation and performance, J. Membr. Sci. 310 (2008) 289–295.

[45] H. Mahdavi, M. Moslehi, A new thin film composite nanofiltration membrane based on PET nanofiber support and polyamide top layer: preparation and characterization, J. Polym. Res. 23 (2016) 257.

[46] J. Schaep, B. Van der Bruggen, C. Vandecasteele, D. Wilms, Influence of ion size and charge in nanofiltration, Separ. Purif. Technol. 14 (1998) 155–162.

[47] S. Zhao, Y. Yao, C. Ba, W. Zheng, J. Economy, P. Wang, Enhancing the performance of polyethylenimine modified nanofiltration membrane by coating a layer of sulfonated poly(ether ether ketone) for removing sulfamerazine, J. Membr. Sci. 492 (2015) 620–629.

[48] S.-P. Sun, T.-A. Hatton, S.-Y. Chan, T.-S. Chung, Novel thin-film composite nanofiltration hollow fiber membranes with double repulsion for effective removal of emerging organic matters from water, J. Membr. Sci. 401–402 (2012) 152–162.

[49] L. Yu, Y. Zhang, L. Xu, Q. Liu, B. Borjigin, D. Hou, J. Xiang, J. Wang, One step prepared Janus acid-resistant nanofiltration membranes with opposite surface charges for acidic wastewater treatment, Separ. Purif. Technol. 250 (2020) 117245.

[50] Y. Chen, F. Liu, Y. Wang, H. Lin, L. Han, A tight nanofiltration membrane with multi-charged nanofilms for high rejection to concentrated salts, J. Membr. Sci. 537 (2017) 407–415.